Effect of the Charge State ($z = -1, 0, +1$) on the Nuclear Magnetic Resonance of Monodisperse $Au_{25}[S(CH_2)_2Ph]_{18}^z$ Clusters

Alfonso Venzo,[∥,‡] Sabrina Antonello,[∥] José A. Gascón,[§] Ivan Guryanov,[∥] Richard D. Leapman,[⊥] Neranjan V. Perera,[§] Alioscka Sousa,[⊥] Martina Zamuner,[∥] Alessandro Zanella,[∥] and Flavio Maran[∥,*]

[∥]Department of Chemistry, University of Padova, via Marzolo 1, 35131 Padova, Italy

[‡]ISTM-CNR, via Marzolo 1, 35131 Padova, Italy

[§]Department of Chemistry, University of Connecticut, 55 North EagleVille Road, Storrs, Connecticut 06269, United States

[⊥]National Institute of Biomedical Imaging and Bioengineering, National Institutes of Health, Bethesda, Maryland 20892, United States

Ⓢ *Supporting Information*

ABSTRACT: Monodisperse $Au_{25}L_{18}^0$ (L = $S(CH_2)_2Ph$) and $[n\text{-}Oct_4N^+][Au_{25}L_{18}^-]$ clusters were synthesized in tetrahydrofuran. An original strategy was then devised to oxidize them: in the presence of bis(pentafluorobenzoyl) peroxide, the neutral or the negatively charged clusters react as efficient electron donors in a dissociative electron-transfer (ET) process, in the former case yielding $[Au_{25}L_{18}^+][C_6F_5CO_2^-]$. As opposed to other reported redox methods, this dissociative ET approach is irreversible, easily controllable, and clean, particularly for NMR purposes, as no hydrogen atoms are introduced. By using this approach, the −1, 0, and +1 charge states of $Au_{25}L_{18}$ could be fully characterized by ^1H and ^{13}C NMR spectroscopy, using one- and two-dimensional techniques, in various solvents, and as a function of temperature. For all charge states, the NMR results and analysis nicely match recent structural findings about the presence of two different ligand populations in the capping monolayer, each resonance of the two ligand families displaying distinct NMR patterns. The radical nature of $Au_{25}L_{18}^0$ is particularly evident in the ^1H and ^{13}C NMR patterns of the inner ligands. The NMR behavior of radical $Au_{25}L_{18}^0$ was also simulated by DFT calculations, and the interplay between theory and experiments revealed a fundamental paramagnetic contribution coming from Fermi contact shifts. Interestingly, the NMR patterns of $Au_{25}L_{18}^-$ and $Au_{25}L_{18}^+$ were found to be quite similar, pointing to the latter cluster form as a diamagnetic species.
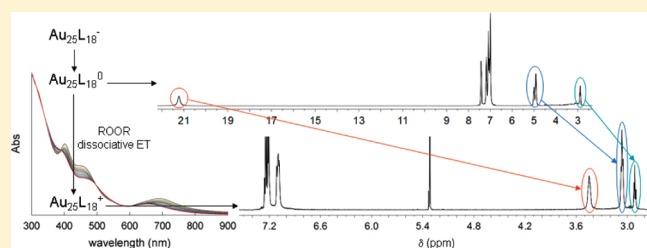
$Au_{25}L_{18}$ is a gold cluster that displays distinct molecule-like redox and optical behaviors. Although studied for some years, leading to a fascinating and intriguing story,[1] it still reserves surprises and challenges from both fundamental and applied viewpoints. Formerly believed to have the $Au_{38}L_{24}$ formula (most studies refer to L = $S(CH_2)_2Ph$ or glutathione), its actual composition has been assessed only recently based on precise mass spectrometry determinations by Tsukuda,[2] Murray,[3] and their co-workers. In its native form, $Au_{25}L_{18}$ bears a negative charge, and its electroneutrality is granted by a counterion, generally the *n*-tetraoctylammonium cation used as the phase-transfer agent in Brust-type syntheses.[4,5] The structure of $[n\text{-}Oct_4N^+][Au_{25}L_{18}^-]$, described in 2008 by both Murray's[6] and Jin's[7] groups, revealed the same surprising features previously reported for $Au_{102}L_{44}$ (L = *p*-mercaptobenzoic acid).[8] For $Au_{25}L_{18}$, there is a core composed of a Au_{13} icosahedron capped by six Au_2L_3 staple-like elements. The latter Au atoms are stellated on 12 faces of the Au_{13} core. According to this structure, the 18 capping ligands belong to either a family of 6 "outer" ligands, where each sulfur atom is connected to two stellated Au atoms, or a family of 12 "inner" ligands, where the sulfur atom is connected to one stellated Au atom and one core Au atom. Figure 1 illustrates the main features of the $Au_{25}L_{18}$ structure.

Some properties of the corresponding neutral $Au_{25}L_{18}$ clusters, obtained by chemical or electrochemical oxidation of $Au_{25}L_{18}^-$, were also described although in former papers they were erroneously assigned, including by us,[9,10] to $Au_{38}L_{24}^+$.[11] Electron-transfer (ET) characterization of the native cluster showed that Au_{25} behaves in all regards as a "simple" molecular redox species,[10,12,13] and its potential can be varied by proper substitution of the capping ligands.[9,14] Establishing the actual structures of the 0 and −1 forms[6,7,15] of Au_{25} has surely been a key step toward our understanding of their physicochemical properties. Density functional theory (DFT) calculations can also be useful: in particular, Akola et al.[16] could successfully predict the "staple" structural motif independently evidenced by the X-ray structure. DFT calculations based on simplified ligands, such as SMe[16] and SH,[17] showed that the three highest occupied molecular orbitals (HOMO) are essentially degenerate. The same degeneracy is apparently valid also for the more complex $S(CH_2)_2Ph$ ligand.[18] On the other hand, although previous calculations indicated that the structural and energetic properties

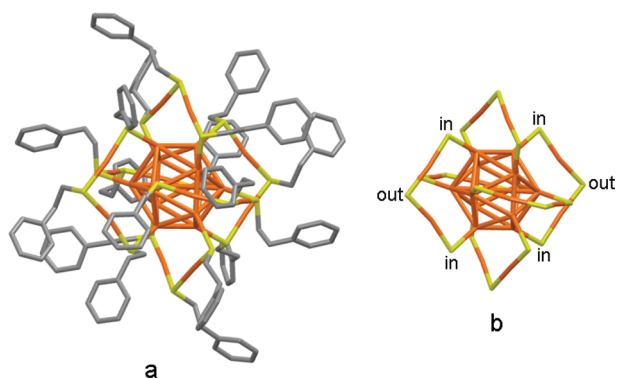**Figure 1.** (a) Depiction of the structure of $Au_{25}[S(CH_2)_2Ph]_{18}$. Gold, sulfur, and carbon are shown in orange, yellow, and gray, respectively; for clarity, hydrogen atoms are not shown. (b) To better appreciate the staple motif and where the two types of ligand are bound, only gold and sulfur atoms are shown; some sulfur atoms belonging to inner (in) and outer (out) ligands have been labeled.

depend weakly on the actual size of the ligand,[19] a very recent DFT study by Aikens, who focused on Au_{25} capped by para-substituted thiophenolate ligands, evidenced that the energy of one of the HOMOs is higher by 0.12−0.13 eV.[20] That the 0 form is paramagnetic has been experimentally verified by electron paramagnetic resonance measurements.[21]

Some important aspects of the physical chemistry of Au_{25} species, however, are still unclear or even unknown. One of them is the dependence of the Au_{25}'s NMR peaks on the charge state. In the following we will focus on $L = S(CH_2)_2Ph$. Murray and co-workers have shown that the ^1H and ^{13}C NMR spectra of $[n\text{-}Oct_4N^+][Au_{25}L_{18}^-]$ display peaks for the phenyl protons and the methylene protons in positions α or β (α and β refer to the position relative to the sulfur atom).[13] In keeping with the evidence stemming from the X-ray structure, the chemical shifts also depend on the actual binding position of L on the gold nanoparticle surface. In CD_2Cl_2, $Au_{25}L_{18}^-$ shows a broad peak at ~3.17 ppm that was assigned to the $\alpha\text{-}CH_2$ of both ligand types. Upon progressive oxidation to the 0 state, this peak undergoes a noticeable downfield shift eventually yielding, for full conversion to the 0 form, a peak at 5.13 ppm. For $Au_{25}L_{18}^-$, the $\beta\text{-}CH_2$ protons of one ligand type are at 2.99 ppm (triplet). For the second ligand group, the $\beta\text{-}CH_2$ protons have been associated with a very broad resonance at lower fields: spectra were shown in which the chemical shift is either at ~3.8 or ~3.65 ppm. This peak broadens and then collapses when a small percentage of the Au_{25} cluster is oxidized. Importantly, for the −1 form the integrals of the $\alpha\text{-}CH_2$ and $\beta\text{-}CH_2$ peaks are each 2/5 of the phenyl resonances: in other words, all peaks, either overlapped or resolved and independently of their actual nature, are present in the spectrum.

Although compelling evidence was provided about the existence of two different types of thiolate binding sites, the authors also concluded that a full interpretation of the splitting and broadening of the $\beta\text{-}CH_2$ resonances could not be attained.[13] Concerning the ^{13}C NMR spectra of $Au_{25}L_{18}^0$ and $Au_{25}L_{18}^+$, obtained by progressive positive charging of the native $Au_{25}L_{18}^-$ cluster with $Ce(SO_4)_2$, the spectra showed that the relevant peaks become somehow scattered and then begin to coalesce with respect to the native cluster.[22] Intriguingly enough, the ^{13}C NMR spectrum of $Au_{25}L_{18}^-$ did not apparently show the expected integral difference between the two ligand populations.

Here we address these and additional issues. Monodisperse $Au_{25}L_{18}^0$ clusters were prepared and studied in detail by ^1H and ^{13}C NMR spectroscopy, using one- and two-dimensional techniques, in various solvents, and as a function of temperature. The results led us to complete a fascinating picture of the NMR behavior of $Au_{25}L_{18}^0$ and also allowed us to gain important insights into that of $Au_{25}L_{18}^-$. The NMR behaviors of the inner and outer $S(CH_2)_2Ph$ ligands of radical $Au_{25}L_{18}^0$ were also simulated by DFT calculations, leading to a remarkable agreement with the experimental outcome. Finally, we devised a strategy, based on dissociative electron transfer,[23,24] for obtaining pure samples of $Au_{25}L_{18}^+$. For all charge states, the NMR results show that the two ligand families display distinct behaviors. The paramagnetic nature of $Au_{25}L_{18}^0$ is particularly evident in the ^1H and ^{13}C NMR patterns of the inner ligands, nicely supported by DFT calculations of the electronic spin density. On the other hand, the behaviors of $Au_{25}L_{18}^-$ and $Au_{25}L_{18}^+$ are quite similar, pointing to the latter species as a diamagnetic species.

■ EXPERIMENTAL SECTION

Chemicals. All reagents were commercially available. Full details of the syntheses of bis(pentafluorobenzoyl) peroxide and $Au_{25}(SCH_2CH_2Ph)_{18}$ are provided in the Supporting Information.

Nuclear Magnetic Resonance. ^1H and ^{13}C NMR spectra were obtained with Bruker model Avance DMX-600 MHz (operating at 600.09 and 150.61 MHz, respectively) and Bruker model Avance DRX-400 MHz (operating at 400.13 and 100.61 MHz, respectively) spectrometers. Chemical shifts (δ) are given as ppm downfield from tetramethylsilane, added to each solvent as the internal standard. Further details and the definitions of the NMR acronyms are in the Supporting Information.

Computational Methods. Spin-unrestricted density functional theory calculations were carried out using the available X-ray structure of $Au_{25}L_{18}^0$ as the starting point.[15] Geometry optimizations were carried out using the software Jaguar (Jaguar, version 7.6, Schrödinger, LLC, New York, NY) with the hybrid functional B3LYP and the LACVP pseudopotential treatment for gold and basis set 6-31 g* for all other atoms. On the energy-minimized structure, NMR parameters were calculated using the software Gaussian 09 (see Supporting Information) with the hybrid functional B3LYP and the LANL2DZ pseudopotential treatment for gold and basis set 6-31 g** for all other atoms. Shielding and isotropic coupling constants were computed using the gauge-including atomic orbitals (GIAOs) formalism as implemented in Gaussian 09.

■ RESULTS AND DISCUSSION

Synthesis and Redox Reactions. The synthesis of monodisperse $Au_{25}L_{18}^0$ clusters was carried out in tetrahydrofuran along similar lines as described by Wu et al.[25] and Dharmaratne et al.[26] The synthesis of $[n\text{-}Oct_4N^+][Au_{25}L_{18}^-]$ was carried out with the same method but in the presence of purposely added $n\text{-}Oct_4NBr$, which stabilizes the −1 form. Monodispersity was evaluated by matrix-assisted laser desorption ionization time-of-flight (MALDI-TOF) mass spectrometry, high-angle annular dark-field scanning transmission electron microscopy (HAADF-STEM), and UV−vis absorption spectroscopy (Supporting Information text and Figures S1 and S2).
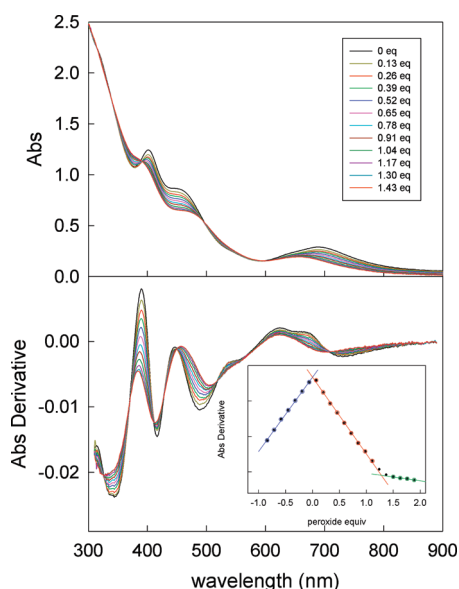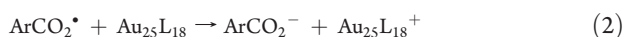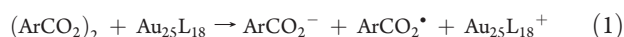
Figure 2. Effect of the addition of bis(pentafluorobenzoyl) peroxide on the UV−vis absorbance spectrum (upper graph) and corresponding derivative (lower graph) of 0.023 mM $Au_{25}L_{18}{}^0$ in CH_2Cl_2 (see text). The inset of the lower graph refers to the plot of the absorbance derivative at 390 nm as a function of the peroxide equivalents (in this case starting from a solution also containing $Au_{25}L_{18}{}^-$: see text); the zero was arbitrarily set at the point corresponding to pure $Au_{25}L_{18}{}^0$.

For the synthesis of $Au_{25}L_{18}{}^+$, we devised a different and cleaner strategy than the aqueous $Ce(SO_4)_2$ oxidation approach[22] or that based on uncontrolled oxidation of the cluster under aerobic conditions,[27] approaches that both lead to poorly resolved NMR or UV−vis spectra. Because we aimed to obtain uncomplicated ^1H and ^{13}C NMR spectra, the oxidant was required (i) to be soluble in the same solvents as $Au_{25}L_{18}{}^0$, (ii) to bear no protons, and (iii) to generate a diamagnetic species; finally, (iv) we required the redox reaction to be quantitative, irreversible, and with clearly identifiable products and counterions. Concerted dissociative ETs are intrinsically irreversible reactions in which an acceptor undergoes cleavage of a frangible bond upon ET.[23,28] Because of their very small BDFE values, peroxides are ideal dissociative-type acceptors,[24,29] and particularly facile reductions occur with peroxides in which the leaving group is a benzoate-type anion.[24] After checking possible candidates, we focused on perfluorodibenzoyl peroxide, $(ArCO_2)_2$, which undergoes a two-electron reduction at quite high potentials (peak potential = 0.50 V vs SCE at 0.1 V s^{-1} in CH_2Cl_2) to form two corresponding benzoate anions.[30] The reaction of the peroxide with $Au_{25}L_{18}$ (eqs 1 and 2) occurs readily upon mixing.

$$(ArCO_2)_2 + Au_{25}L_{18} \rightarrow ArCO_2{}^- + ArCO_2{}^\bullet + Au_{25}L_{18}{}^+ \qquad (1)$$

$$ArCO_2{}^\bullet + Au_{25}L_{18} \rightarrow ArCO_2{}^- + Au_{25}L_{18}{}^+ \qquad (2)$$

In principle, reaction 2 is in competition with the spontaneous decarboxylation of the benzoyloxy radical. In a nonreactive solvent, the lifetime of benzoyloxy radicals is on the order of microseconds and the decarboxylation rate constant is mildly influenced by ring substituents:[31] a reasonable estimate for the decarboxylation rate constant of $(ArCO_2)_2$ is thus ca. $1 \times 10^6 s^{-1}$.

Since reaction 2 is diffusion controlled,[30] decarboxylation should not compete with ET down to millimolar concentrations.

The irreversible ET reaction of $(ArCO_2)_2$ with $Au_{25}L_{18}{}^0$ was monitored by UV−vis absorption spectroscopy. The upper graph of Figure 2 shows the progressive change of the absorbance of 0.023 mM $Au_{25}L_{18}{}^0$ in CH_2Cl_2 as a function of the amount of added peroxide. The number of equivalents in the legend refers to the theoretical amount of peroxide required for full conversion of $Au_{25}L_{18}{}^0$ into $Au_{25}L_{18}{}^+$ (two-electron process: sum of reactions 1 and 2). The lower graph of Figure 2 shows the corresponding derivative. Main features marking the transition are as follows: increase of absorbance just before the typical band of $Au_{25}L_{18}{}^0$ at 401 nm; disappearance of the latter; slight increase of absorbance around 530 nm; disappearance of the $Au_{25}L_{18}{}^0$ band at 689 nm to leave a band centered at 659 nm; isosbestic points at 390, 495, and 606 nm. It also is worth noting that after ca. 1.3 equiv of peroxide has been added to the solution, no further transformation occurs. This indicates that under these conditions no further conversion of the cluster to the +2 charge state occurs.

The absorbance derivative at the main isosbestic points is particularly sensitive toward changes of the cluster's redox state. It is worth stressing that whereas some derivatives are sensitive to both the $Au_{25}L_{18}{}^- \rightarrow Au_{25}L_{18}{}^0$ and $Au_{25}L_{18}{}^0 \rightarrow Au_{25}L_{18}{}^+$ transitions, others essentially feel only one of the two conversions. The inset of the lower graph of Figure 2 shows how the derivative at 390 nm changes upon stepwise addition of the peroxide to a CH_2Cl_2 solution of the cluster. Because of the progressive change of the position of the derivative maximum, the plots are best appreciated starting from a (partially oxidized) solution of the −1 charge state. Figure 2 nicely highlights the presence of two breaks. Whereas the first corresponds to full conversion of $Au_{25}L_{18}{}^-$ into $Au_{25}L_{18}{}^0$, the second occurs after further addition of ca. 1.3 equiv and is associated with conversion of $Au_{25}L_{18}{}^0$ into $Au_{25}L_{18}{}^+$. The absorbance derivative at 496 nm or the absorbance at 369 or 401 nm gave virtually identical results. The titration curve of Figure 2 thus shows that the ET reaction 2 is not quantitative because given the low Au_{25} concentration employed, 0.023 mM, decarboxylation partially competes. This is in keeping with the above considerations concerning the lifetime of the benzoyloxy radical. On the other hand, this also ensures that at the millimolar concentrations typically used in, for example, electrochemistry (1 mM) and NMR (3 mM) experiments, bis(pentafluorobenzoyl) peroxide is an excellent and quantitative two-electron ET acceptor for carrying out a fast and controlled transformation of either $Au_{25}L_{18}{}^-$ into $Au_{25}L_{18}{}^0$ or $Au_{25}L_{18}{}^0$ into $Au_{25}L_{18}{}^+$.

A final comment concerns the shift of the onset of optical absorbance upon oxidation. From the absorbance onset, the HOMO−LUMO gap of $Au_{25}L_{18}{}^-$ was evaluated to be 1.33 eV.[32] The changes observed on the low energy side of the spectrum show that when $Au_{25}L_{18}{}^-$ is oxidized to radical $Au_{25}L_{18}{}^0$, the gap increases, as already discussed.[33] From Figure S2 we estimate this increase to be ca. 0.16 eV. According to the spectra of Figure 2, oxidation to $Au_{25}L_{18}{}^+$ appears to further increase the gap to as much as 1.53 eV, which suggests that absorption now involves an orbital lower in energy by 0.2 eV with respect to the HOMO of $Au_{25}L_{18}{}^-$.

^1H and ^{13}C NMR Spectroscopy of $Au_{25}L_{18}{}^z$. ^1H and ^{13}C NMR spectroscopy measurements were carried out in different solvents (dichloromethane-d_2, benzene-d_6, toluene-d_8, 1,2-dichloroethane-d_4) and as a function of temperature, depending
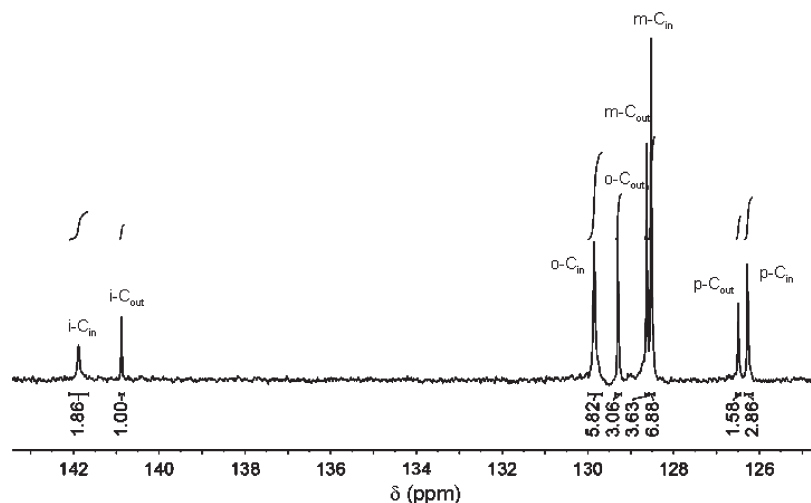
Figure 3. ^{13}C NMR spectrum of 3 mM $[n\text{-Oct}_4N^+][Au_{25}L_{18}{}^-]$ in dichloromethane-d_2 at 298 K. The spectrum pertains to the region of aromatic carbons (the full spectrum is in Figure S4).

on the cluster oxidation state or for highlighting specific features of the differently charged clusters. In the following we will use the subscripts "out" to label the resonances of the 6 outer ligands and "in" to indicate those of the 12 inner ligands. According to the work of Parker et al.,[13] the chemical shifts of the CH_2 groups of the two ligand families in $Au_{25}L_{18}{}^-$ are different and so are their sensitivities toward the presence of oxidized clusters, $Au_{25}L_{18}{}^0$. Upon progressive oxidation to the 0 state, while the α-CH_2 peak, attributed to the overlap of the contribution of both inner and outer ligands, was described to undergo a downfield shift from 3.17 to 5.13 ppm, the 3.65−3.8 ppm broad resonance attributed to β-$(CH_2)_{in}$ disappears. We started by revisiting the ^{1}H and ^{13}C NMR behavior of $[n\text{-Oct}_4N^+][Au_{25}L_{18}{}^-]$ in dichloromethane-d_2. Heteronuclear correlation analysis (for the HMBC spectrum and details, see Supporting Information Figure S3) showed that whereas the triplet at 2.93 ppm pertains to $(\beta$-$CH_2)_{out}$, as already assigned,[13] the complex peak centered at ca. 3.1 ppm is, in fact, due to the overlap of the $(\alpha$-$CH_2)_{out}$ and $(\beta$-$CH_2)_{in}$ resonances. The remaining broad peak at ca. 3.8 ppm is thus due to $(\alpha$-$CH_2)_{in}$. Concerning the ^{13}C NMR behavior, we found that for both aryl and alkyl carbons the two ligand types exhibit distinct resonances and the integrals are in very good agreement with the expected inner-to-outer ligand 2:1 ratio. This is shown in Figure 3 for the aryl carbons (Supporting Information Figure S4 shows the whole ^{13}C spectrum). The relevant ^{1}H and ^{13}C NMR data of $[n\text{-Oct}_4N^+][Au_{25}L_{18}{}^-]$ are gathered in Supporting Information Tables S1 and S2, respectively.

Progressive oxidation of $Au_{25}L_{18}{}^-$ proceeds as already described for some of the peaks by Murray's group.[13] As expected based on the unpaired electron of $Au_{25}L_{18}{}^0$, its NMR behavior is quite complex. In the following, all assignments are the result of homo- and heteronuclear 2D correlation spectra (for details, see Supporting Information). Figure 4 shows the ^{1}H NMR spectra of $Au_{25}L_{18}{}^0$ in dichloromethane-d_2 and toluene-d_8. In CD_2Cl_2 (298 K), the $(\beta$-$CH_2)_{out}$ resonance appears as a triplet at 2.81 ppm, which compares well with the corresponding $(\beta$-$CH_2)_{out}$ triplet of $Au_{25}L_{18}{}^-$ at 2.93 ppm and that of the free ligand at 3.00 ppm. No significant solvent effect was noticed (cf., Table S1). The second β-CH_2 resonance, $(\beta$-$CH_2)_{in}$, occurs as a broad peak at 5.25 ppm, i.e., slightly downfield relative to the better resolved $(\alpha$-$CH_2)_{out}$ peak at 5.17 ppm. A very similar situation was
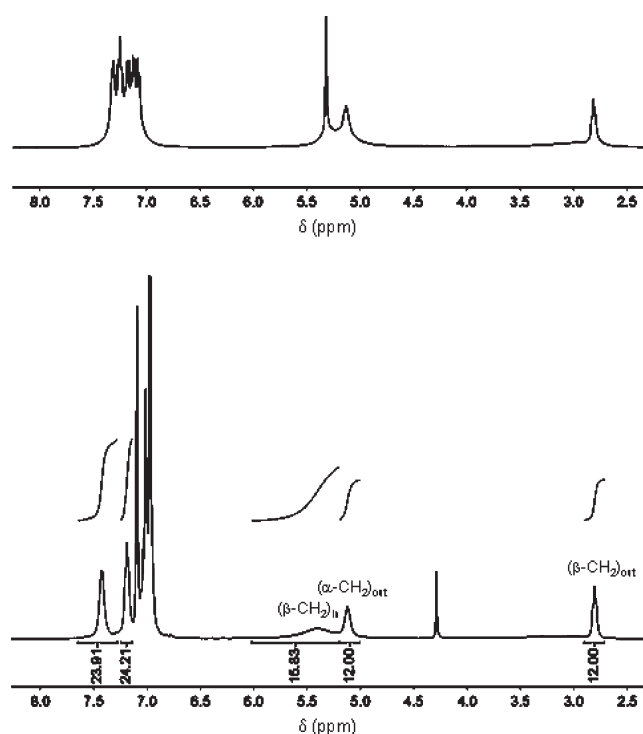

Figure 4. ^{1}H NMR spectra of monodisperse 3 mM $Au_{25}L_{18}{}^0$ in dichloromethane-d_2 (upper graph) and toluene-d_8 (lower graph) at 298 K. The peaks at 5.33 ppm (upper graph) and 4.29 ppm (lower graph) are due to CH_2Cl_2 impurities.

observed in other solvents. This means that as one goes from $Au_{25}L_{18}{}^-$ to $Au_{25}L_{18}{}^0$, both the $(\beta$-$CH_2)_{in}$ and $(\alpha$-$CH_2)_{out}$ peak undergo a quite significant downfield shift. Interestingly, in aromatic solvents the $(\beta$-$CH_2)_{in}$ resonance shifts more downfield and becomes slightly sharper with respect to the behavior in chlorinated solvents. We also noted that in the former solvent type, all peaks are generally better resolved.

As shown in the lower graph of Figure 4, whereas the integrals of the $(\alpha$-$CH_2)_{out}$ and $(\beta$-$CH_2)_{out}$ peaks are, as expected, identical and exactly half the value of the peak corresponding

Figure 5. ^{1}H NMR spectrum of monodisperse 3 mM $Au_{25}L_{18}^0$ in toluene-d_8 as a function of temperature. For the sake of better comparison, the spectra only show the region from 2.5 to 6.5 ppm. In the inset the NOESY spectrum at 358 K shows both negative (green) and positive (violet) cross-peaks.

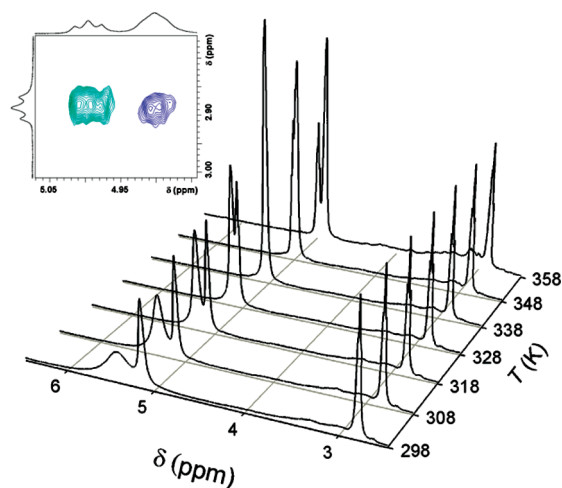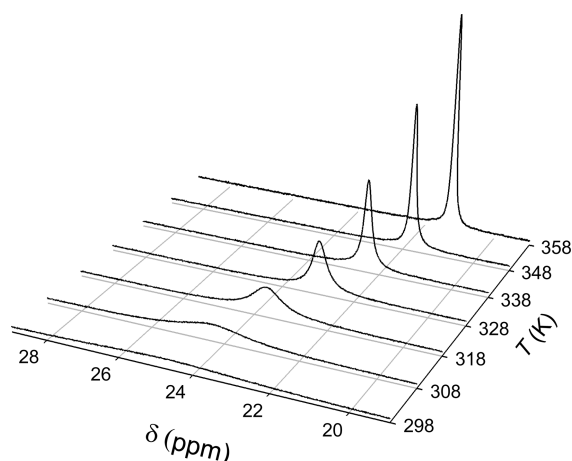**Figure 6.** ^{1}H NMR spectrum of monodisperse 3 mM $Au_{25}L_{18}^0$ in toluene-d_8 as a function of temperature. For the sake of better comparison, the spectra only show the $(\alpha\text{-}CH_2)_{in}$ zone.

to the o- or p-hydrogen resonances of the inner ligands (see below), the integral of the $(\beta\text{-}CH_2)_{in}$ peak is less than twice. This difference, however, is related to temperature: Figure 5 shows that the $(\beta\text{-}CH_2)_{in}$ peak becomes sharper and undergoes a sizable upfield shift as the temperature increases. Eventually, its integral becomes twice the value of the $(\alpha\text{-}CH_2)_{out}$ peak: from 298 to 358 K (toluene-d_8) the ratio between the integrals of $(\beta\text{-}CH_2)_{in}$ and $(\alpha\text{-}CH_2)_{out}$ resonances smoothly increases from 1.32 to 1.99. As the temperature increases, the $(\alpha\text{-}CH_2)_{out}$ peak develops into a more resolved triplet and its position barely changes; similarly, the $(\beta\text{-}CH_2)_{out}$ resonance is almost unaffected by temperature. The spectra of Figure 5 pertain to toluene-d_8, but similar results were observed in benzene-d_6. Overall, these results show that the $\alpha\text{-}CH_2$ resonance previously described[13] to undergo a downfield shift from 3.13 to 5.17 ppm (δ values refer to our own determinations: see Table S1) upon progressive oxidation of $Au_{25}L_{18}^-$ only belongs to the outer ligands. A final comment about the temperature effect on the $(\beta\text{-}CH_2)_{in}$ and

$(\alpha\text{-}CH_2)_{out}$ resonances concerns the observation of a chemical exchange occurring between the $(\beta\text{-}CH_2)_{in}$ and $(\beta\text{-}CH_2)_{out}$ peaks at high temperatures. This was clearly detected in the phase-sensitive NOESY spectrum (inset of Figure 5) and points to a quite dynamic situation attained in this condition by the ligands in the cluster. It is conceivable that this exchange phenomenon could be responsible for the effects observed upon annealing similar clusters at 80 °C.[34,35]

The most intriguing resonance is that of $(\alpha\text{-}CH_2)_{in}$. In the ^{1}H NMR spectrum of $Au_{25}L_{18}^-$ this resonance, now established to be that at 3.8 ppm, disappears as soon as the cluster is partially oxidized. However, in the usual ^{1}H NMR spectral window we could not find any trace of it, neither by increasing or decreasing the temperature. In the latter experiment, carried out in CD_2Cl_2, we only noticed a progressive broadening of all resonances. The $(\alpha\text{-}CH_2)_{in}$ resonance, however, was clearly detected using toluene-d_8 and 1,2-dichloroethane-d_4 as the solvents, which allowed us to increase the temperature to 358 and 348 K, respectively. At 298 K and in both solvents, the $(\alpha\text{-}CH_2)_{in}$ resonance is indeed barely detectable and very broad (the full width at half-maximum, fwhm, is ca. 2100 and 1800 Hz, respectively) and occurs at very low fields, i.e., 24.9 and 24.4 ppm, respectively. Upon increasing the temperature, the peak sharpens (in toluene-d_8 at 358 K, fwhm is 53 Hz; in 1,2-dichloroethane-d_4 at 348 K, fwhm is 67 Hz) and undergoes a significant upfield shift (Figure 6): from 298 to 358 K, its position shifts by as much as, for example, 3.68 ppm in toluene-d_8. Correspondingly, its integral smoothly increases, and at 358 K, it is already 1.66 times larger than that of either $(\alpha\text{-}CH_2)_{out}$ or $(\beta\text{-}CH_2)_{out}$ resonances (Supporting Information Figure S5). Unfortunately, the broadness of both $(\alpha\text{-}CH_2)_{in}$ and $(\beta\text{-}CH_2)_{in}$ peaks rules out the possibility of obtaining COSY cross-peaks even at high temperature. In this context, the outcome of the DFT calculations (see below) was particularly useful to provide further support to our assignment.

Comparison of all integrals thus provides quantitative assessment of the presence and relative numbers of ligand types in the capping monolayer of $Au_{25}L_{18}^0$. It is evident that the chemical shift value of the $\alpha\text{-}CH_2$ resonance of the inner ligands undergoes a particularly dramatic change when the cluster charge is varied from -1 to 0. This behavior is attributed to the contact interaction of the nuclear magnetic moments with the unpaired electron, which further confirms that $Au_{25}L_{18}^0$ is a paramagnetic species. Whereas the effect of this interaction is very significant for the ^{1}H nuclei nearer to the gold core, $(\alpha\text{-}CH_2)_{in}$, it is still quite evident for either $(\beta\text{-}CH_2)_{in}$ or $(\alpha\text{-}CH_2)_{out}$ but is undetectable for $(\beta\text{-}CH_2)_{out}$.

Analysis of the ^{1}H NMR phenyl region, in comparison with the behavior of $Au_{25}L_{18}^-$, also led to surprises. For $Au_{25}L_{18}^-$ in CD_2Cl_2, the o-, m-, and p-proton resonances are in the 7.0—7.2 ppm region; they largely overlap, and assignments could be possible through careful inspection of the homo- and heteronuclear correlation experiments: the relevant TOCSY and ROESY spectra are in Supporting Information Figures S10 and S11, and the HMQC and HMBC spectra are in Supporting Information Figures S12 and S13. For $Au_{25}L_{18}^0$, the aryl proton resonances of the inner ligands are at 7.32 (o-H) and 7.25 (m-H). On the other hand, a somehow different outcome was observed in aromatic solvents, also in terms of resolution of the peaks of inner and outer ligands. In C_6D_6 (298 K), whereas the resonances of the peaks of the o-, m-, and p-protons of the outer ligands are at 6.99, 7.05, and 6.97 ppm, the corresponding values
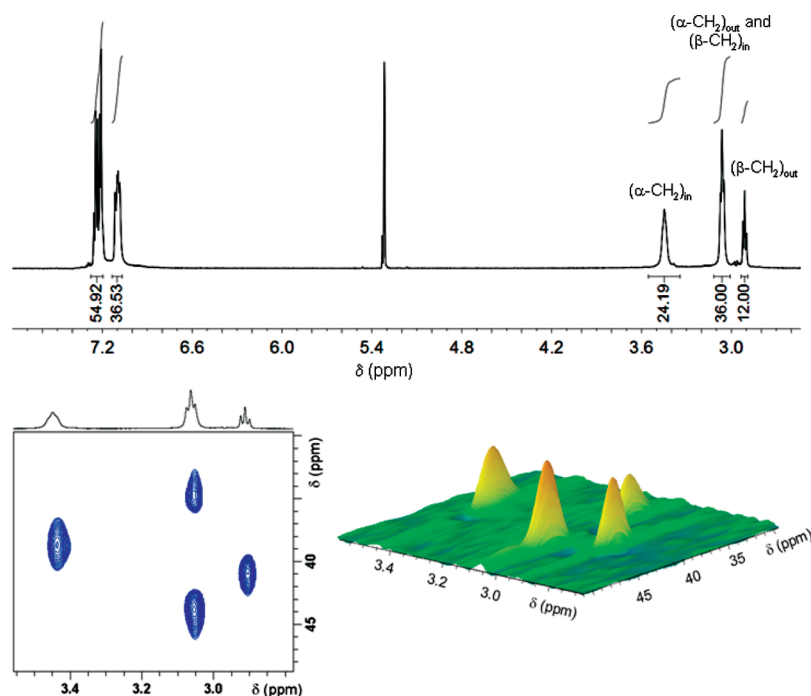
Figure 7. ^{1}H NMR spectrum of 3 mM $Au_{25}L_{18}^{+}$ (upper graph) obtained by quantitative oxidation of monodisperse $Au_{25}L_{18}^{0}$ in dichloromethane-d_2 at 298 K. The HMQC spectrum is shown in the lower graphs as either a 2D (left) or 3D plot (right). The peak at 5.33 ppm is due to CH_2Cl_2.

of the inner ligands are 7.46, 7.20, and 6.99 ppm. Therefore, a noticeable effect is brought about by C_6D_6 particularly on the o-H of the inner ligands; the effect of toluene-d_8 on o-H is similar, though slightly smaller (7.42 ppm). The o-H peak is broad but develops into a doublet when the temperature increases (cf., Supporting Information Figure S6). That the position of the o-H peak of the inner ligands is strongly solvent dependent is nicely evidenced when an equimolar solution of $Au_{25}L_{18}^{0}$ in CD_2Cl_2 is added in progressively increasing amounts to a C_6D_6 solution, thereby causing the o-CH peak to shift upfield quite rapidly (Supporting Information Figure S7). This particular sensitivity of some resonances of the inner ligands on the type of solvent (aromatic vs chlorinated) is indeed worth noting.

The main features of the ^{13}C NMR spectrum of $Au_{25}L_{18}^{0}$ (Supporting Information Figures S8 and S9) are, once again, the evidence of two ligand populations in different amounts and with different chemical shifts. Interestingly, the chemical shifts of the inner ligands are slightly downfield relative to the corresponding carbons of the outer ligands which, in turn, are more similar to the values of the free ligand $Ph(CH_2)_2SH$ (Table S2). The downfield shift effect is particularly marked for the ortho and ipso carbons, which are nearer to the gold core. The resonances of the two alkyl carbons are particularly interesting. Both $(\alpha\text{-C})_{out}$ and $(\beta\text{-C})_{out}$ peaks are markedly shifted downfield relative to the free ligand. On the other hand, the effect of paramagnetism is huge for the inner ligands (Supporting Information Figures S14 and S15), the observed resonances being at -134 and $+350$ ppm (358 K, toluene-d_8); the corresponding fwhm values are ca. 4500 and 8000 Hz. Since based on the experimental results no satisfactory assignment could be made, the attribution of the chemical shifts of $(\alpha\text{-C})_{in}$ and $(\beta\text{-C})_{in}$ (cf., Table S2) was inferred from the outcome of the DFT calculations.

^{1}H and ^{13}C NMR spectra of $[Au_{25}L_{18}^{+}][C_6F_5CO_2^{-}]$ were obtained in CD_2Cl_2 at 298 K (Figures 7 and Supporting Information S16). As we already saw, at millimolar concentration

the +1 form is obtained quantitatively by reaction of $Au_{25}L_{18}^{0}$ with 1 ET equiv of bis(pentafluorobenzoyl) peroxide. Upon addition of the latter, the most significant changes observable in the ^{1}H NMR spectrum of $Au_{25}L_{18}^{0}$ are the disappearance of the peaks that underwent a large change in the conversion $Au_{25}L_{18}^{-} \rightarrow Au_{25}L_{18}^{0}$, i.e., those corresponding to the $(\alpha\text{-CH}_2)_{in}$, $(\beta\text{-CH}_2)_{in}$, and $(\alpha\text{-CH}_2)_{out}$ resonances. Figure 7 shows that beside the peaks in the phenyl region there are only three visible resonances at 3.45, 3.06, and 2.91 ppm with relative integrals in ratio 2:3:1. The last peak is easily assigned to the $(\beta\text{-CH}_2)_{out}$ resonance which we already saw to be essentially the same in the free ligand and in the gold nanoparticle, independently of its charge state. The COSY spectrum (Supporting Information Figure S17) shows that this peak correlates with the peak at 3.06 ppm, and thus the latter is partially due to the $(\alpha\text{-CH}_2)_{out}$ resonance. According to the values of the three integrals, this also implies that the latter and one of the two $(CH_2)_{in}$ resonances have essentially the same chemical shift. On the basis of the TOCSY spectrum (Supporting Information Figure S18), this resonance is identified as due to $(\beta\text{-CH}_2)_{in}$ which, similarly to $(\beta\text{-CH}_2)_{out}$, correlates with the ortho and meta aromatic protons. In keeping with the values of the three integrals, the remaining peak, at 3.45 ppm, is thus due to $(\alpha\text{-CH}_2)_{in}$. Therefore, we can conclude that the chemical shifts of the methylene resonances of $Au_{25}L_{18}^{+}$ very much resemble those of $Au_{25}L_{18}^{-}$.

The ^{13}C NMR resonances of the corresponding carbon atoms could be assessed based on the HMQC results (Figure 7). The ratio between the corresponding 3D integrals of $(\alpha\text{-CH}_2)_{in}$, $(\beta\text{-CH}_2)_{in}$, $(\alpha\text{-CH}_2)_{out}$, and $(\beta\text{-CH}_2)_{out}$ are 1: 0.9: 0.6: 0.6. Because these peaks refer to groups with the same correlation constants but slightly different relaxation times, they can be cautiously used to distinguish the α-C from the β-C resonance.
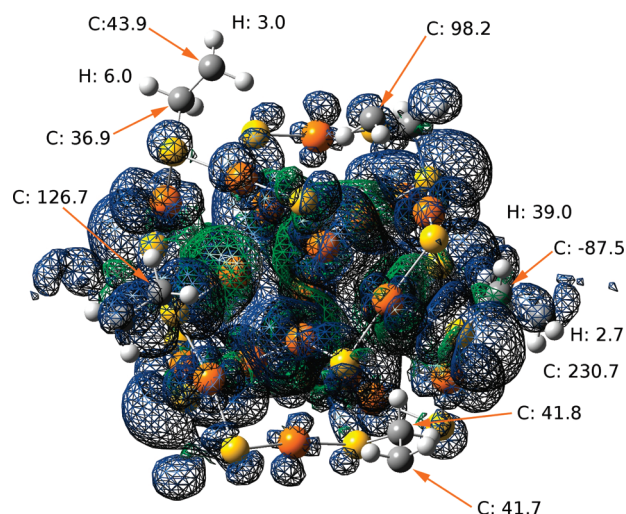
Figure 8. Isosurface of the electronic spin density (isovalue = 0.0001). Blue and green surfaces correspond to α and β spin, respectively. For clarity, only some of the ethyl groups are shown, and phenyl groups are not displayed. Gold, sulfur, carbon, and hydrogen atoms are shown in orange, yellow, gray, and white, respectively. Typical values of calculated chemical shifts at 298 K are shown.

Concerning the phenyl region, the TOCSY spectrum of $[\text{Au}_{25}\text{L}_{18}{}^{+}][\text{C}_6\text{F}_5\text{CO}_2{}^{-}]$ shows cross-peaks between *o*- and *m*-CH groups of outer and inner ligands (Figure S18) and leads to the identification of all resonances (Table S1). The integrals of the phenyl and methylene regions match very nicely (Figure 7). Interestingly, we note that the chemical shifts of the inner and outer *o*-CH resonances are appreciably upfield with respect to the others. The sensitivity of some resonances of the inner ligands to the cluster charge state is indeed worth noting: this is the case of *p*-CH of $\text{Au}_{25}\text{L}_{18}{}^{-}$ and the *o*-CH of both $\text{Au}_{25}\text{L}_{18}{}^{0}$ and $\text{Au}_{25}\text{L}_{18}{}^{+}$, although downfield and upfield, respectively. The ^{13}C spectrum of $[\text{Au}_{25}\text{L}_{18}{}^{+}][\text{C}_6\text{F}_5\text{CO}_2{}^{-}]$ (Figure S16) is not as spectacular as those of the -1 and 0 forms (Figures 2, S8, and S9), mainly because the +1 redox state is less stable than the other redox states (we observed that overnight some transformation of the NMR sample occurred). Heteronuclear 2D correlation experiments (cf., Supporting Information Figures S19 and S20), however, allowed us to assign all aliphatic and aromatic resonances.

DFT Evaluation of $\text{Au}_{25}\text{L}_{18}{}^{0}$ NMR. Because of the critical radical nature of $\text{Au}_{25}\text{L}_{18}{}^{0}$ and the rich features of its NMR spectrum, we focused our calculations on the NMR parameters of this cluster. Calculations were performed in vacuum and thus can be compared with the NMR data obtained in solvents of low dielectric constant (i.e., toluene). Calculations give sound support to the observation that ^{1}H and ^{13}C NMR present different features for inner and outer ligands and provide further insight into the origin of the various resonances and their temperature dependence (Supporting Information Tables S3–S5). Unless otherwise specified, all calculations refer to 298 K. An immediate observation that arises from the calculations concerns the extent of delocalization of the spin density. A measure of this delocalization is to consider the spin density on the $(\alpha\text{-CH}_2)$. Whereas the average spin density on $(\alpha\text{-CH}_2)_{\text{in}}$ is $0.0008 \times \hbar/2$, that of $(\alpha\text{-CH}_2)_{\text{out}}$ is $0.00007 \times \hbar/2$, i.e., 1 order of magnitude smaller. Figure 8 provides a visual representation of such a large difference between inner and outer ligands. For a spin isosurface of

$0.0001 \times \hbar/2$, no spin density is evident for outer ligands. This translates into a uniform set of chemical shifts in the region 33–46 ppm. For inner ligands, the spin density clearly extends up to the $(\beta\text{-CH}_2)$ and, for some ligands, even to the phenyl groups. Interestingly, a closer inspection of the spin density of inner ligands (Figure 8, Supporting Information Figures S23 and S24) shows that it presents a nonuniform distribution. For instance, an excess of α spin can give rise to values ranging from 30 to 130 ppm for $(\alpha\text{-C})_{\text{in}}$ and from 40 to 260 ppm for $(\beta\text{-C})_{\text{in}}$. On the other hand, an excess of β spin, which only extends up to the $(\alpha\text{-C})_{\text{in}}$ is uniquely responsible for the negative chemical shifts. All these observation are consistent with the experimental data presented in Table S2. In addition, calculations reveal that the normal band in the 33–46 region, which originates mainly from the outer-ligand alkyl carbon atoms, also has some minor contribution from both $(\alpha\text{-C})_{\text{in}}$ and $(\beta\text{-C})_{\text{in}}$.

Calculations of ^{1}H chemical shifts also show a strong correlation with the extent of spin delocalization as in the case of ^{13}C. That is, outer ligands behave in a remarkably different manner than inner ligands (for representative values, see Figure 8; for all values, see Table S5). Differently from ^{13}C, however, the proton resonances of $(\alpha\text{-CH}_2)_{\text{out}}$ and $(\beta\text{-CH}_2)_{\text{out}}$ present distinct distributions: one centered at $\sim$5.55 ppm and the other at $\sim$3.55 ppm. This agrees very well with the corresponding experimental values of 5.13 ppm and 2.81 ppm (cf., Table S1, toluene-d_8), respectively. $(\alpha\text{-CH}_2)_{\text{out}}$ are also more sensitive to temperature than $(\beta\text{-CH}_2)_{\text{out}}$ (Table S3), experiencing an upfield shift of -0.28 ppm upon increasing the temperature to 358 K, in modest agreement with the experimentally observed shift (-0.08 ppm). Computed chemical shifts for $(\beta\text{-CH}_2)_{\text{in}}$ give rise to a small shift ($+0.07$ ppm), whereas the experimentally observed shift is (-0.5 ppm), suggesting that the extent of spin delocalization is underestimated at the current level of theory. As expected, $(\alpha\text{-CH}_2)_{\text{in}}$ exhibits the most noticeable effect. The computed average is 23.85 ppm at 298 K and 20.6 ppm at 358 K, in excellent agreement with the experimental values measured in toluene-d_8 at these two temperatures (24.9 ppm and 21.22 ppm, respectively). This correspondence clearly demonstrates the paramagnetic behavior of $\text{Au}_{25}\text{L}_{18}{}^{0}$ arising from the Fermi-contact term.

■ CONCLUSIONS

We synthesized $\text{Au}_{25}\text{L}_{18}{}^{0}$ and $[n\text{-Oct}_4\text{N}^{+}][\text{Au}_{25}\text{L}_{18}{}^{-}]$ clusters, capped by phenylethanethiolate ligands, in a monodisperse form. The charge state of the Au_{25} clusters could be precisely controlled by using a smooth oxidant, bis(pentafluorobenzoyl) peroxide, which reacts with the clusters according to an irreversible dissociative ET. This original redox approach works very nicely starting from either $[n\text{-Oct}_4\text{N}^{+}][\text{Au}_{25}\text{L}_{18}{}^{-}]$ or $\text{Au}_{25}\text{L}_{18}{}^{0}$, in the second case yielding $[\text{Au}_{25}\text{L}_{18}{}^{+}][\text{C}_6\text{F}_5\text{CO}_2{}^{-}]$. Because the peroxide and its reduction product do not introduce hydrogen atoms, this dissociative ET provides a particularly convenient approach for NMR purposes.

For the first time, through precise redox control of the charge state of Au_{25} clusters we could fully characterize this cluster by ^{1}H and ^{13}C NMR spectroscopy as a function of its core charge state (-1, 0, and $+1$). Analysis of the NMR spectra $[n\text{-Oct}_4\text{N}^{+}]$-$[\text{Au}_{25}\text{L}_{18}{}^{-}]$ allowed us to refine previous peak assignments and to evidence quantitatively the presence of two families of ligands, in full agreement with the X-ray crystallography structure. The same overall scenario was assessed for monodisperse $\text{Au}_{25}\text{L}_{18}{}^{0}$

but with remarkable chemical-shift differences caused by the paramagnetic nature of this Au_{25} form. We found that the 12 inner ligands are particularly sensitive to the unpaired electron. Comparative analysis of the various resonances led us to show that whereas the $(\beta\text{-}CH_2)_{out}$ resonance is essentially unaffected by the unpaired spin, both the $(\alpha\text{-}CH_2)_{out}$ and $(\beta\text{-}CH_2)_{in}$ resonances are affected and undergo a sizable downfield shift. On the other hand, the $(\alpha\text{-}CH_2)_{in}$ peak undergoes a dramatic downfield shift to ca. 25 ppm. A dramatic effect of paramagnetism is also evident in the ^{13}C NMR spectrum for both $(\alpha\text{-}C)_{in}$ and $(\beta\text{-}C)_{in}$. As for the -1 form, the ^{13}C NMR peaks and integrals confirm the presence of two distinct ligand populations. The paramagnetic behavior of $Au_{25}L_{18}{}^0$, mainly arising from the Fermi-contact term, was nicely confirmed by DFT calculations of chemical shifts, and a clear correlation between the extent of spin delocalization and the nature of the ligands was established. Finally, the NMR behavior of $Au_{25}L_{18}{}^+$ was found to be quite similar to that of $Au_{25}L_{18}{}^-$, with distinct contributions from the two types of ligand. According to our NMR study, we conclude that the positively charged cluster is a diamagnetic species. According to the UV−vis absorption spectra, the HOMO−LUMO gap of $Au_{25}L_{18}{}^+$ is larger by ca. 0.2 eV than that of $Au_{25}L_{18}{}^-$. We believe that the redox methodologies and the results and analyses described here will provide useful tools and guidelines for the study of other monodisperse molecule-like metal clusters.

■ ASSOCIATED CONTENT

ⓢ Supporting Information. Additional ^1H and ^{13}C NMR spectroscopy spectra, 2D correlation spectra, UV−vis absorption spectroscopy spectra, DFT tables and figures. This material is available free of charge via the Internet at http://pubs.acs.org.

■ AUTHOR INFORMATION

Corresponding Author
*E-mail: flavio.maran@unipd.it.

■ ACKNOWLEDGMENT

■ REFERENCES

(1) Parker, J. F.; Fields-Zinna, C. A.; Murray, R. W. *Acc. Chem. Res.* **2010**, *43*, 1289–1296.

(2) Negishi, Y.; Nobusada, K.; Tsukuda, T. *J. Am. Chem. Soc.* **2005**, *127*, 5261–5270.

(3) Tracy, J. B.; Kalyuzhny, G.; Crowe, M. C.; Balasubramanian, R.; Choi, J.-P.; Murray, R. W. *J. Am. Chem. Soc.* **2007**, *129*, 6706–6707.

(4) Brust, M.; Walker, M.; Bethell, D.; Schiffrin, D. J.; Whyman, R. *J. Chem. Soc., Chem. Commun.* **1994**, 801–802.

(5) Donkers, R. L.; Lee, D.; Murray, R. W. *Langmuir* **2004**, *20*, 1945–1952.

(6) Heaven, M. W.; Dass, A.; White, P. S.; Holt, K. M.; Murray, R. W. *J. Am. Chem. Soc.* **2008**, *130*, 3754–3755.

(7) Zhu, M.; Aikens, C. M.; Hollander, F. J.; Schatz, G. C.; Jin, R. *J. Am. Chem. Soc.* **2008**, *130*, 5883–5885.

(8) Jadzinsky, P. D.; Calero, G.; Ackerson, C. J.; Bushnell, D. A.; Kornberg, R. D. *Science* **2007**, *318*, 430–433.

(9) Holm, A. H.; Ceccato, M.; Donkers, R. L.; Fabris, L.; Pace, G.; Maran, F. *Langmuir* **2006**, *22*, 10584–10589.

(10) Antonello, S.; Holm, A. H.; Instuli, E.; Maran, F. *J. Am. Chem. Soc.* **2007**, *129*, 9836–9837.

(11) Murray, R. W. *Chem. Rev.* **2008**, *108*, 2688–2720.

(12) Choi, J.-P.; Murray, R. W. *J. Am. Chem. Soc.* **2006**, *128*, 10496–10502.

(13) Parker, J. F.; Choi, J.-P.; Wang, W.; Murray, R. W. *J. Phys. Chem. C* **2008**, *112*, 13976–13981.

(14) Guo, R.; Murray, R. W. *J. Am. Chem. Soc.* **2005**, *127*, 12140–12143.

(15) Zhu, M.; Eckenhoff, W. T.; Pintauer, T.; Jin, R. *J. Phys. Chem. C* **2008**, *112*, 14221–14224.

(16) Akola, J.; Walter, M.; Whetten, R. L.; Häkkinen, H.; Grönbeck, H. *J. Am. Chem. Soc.* **2008**, *130*, 3756–3757.

(17) Aikens, C. M. *J. Phys. Chem. C* **2008**, *112*, 19797–19800.

(18) Aikens, C. M. *J. Phys. Chem. A* **2009**, *113*, 10811–10817.

(19) Grönbeck, H.; Walter, M.; Häkkinen, H. *J. Am. Chem. Soc.* **2006**, *128*, 10268–10275.

(20) Aikens, C. M. *J. Phys. Chem. Lett.* **2010**, *1*, 2594–2599.

(21) Zhu, M.; Aikens, C. M.; Hendrich, M. P.; Gupta, R.; Qian, H.; Schatz, G. C.; Jin, R. *J. Am. Chem. Soc.* **2009**, *131*, 2490–2492.

(22) Song, Y.; Harper, A. S.; Murray, R. W. *Langmuir* **2005**, *21*, 5492–5500.

(23) Antonello, S.; Maran, F. *Chem. Soc. Rev.* **2005**, *34*, 418–428.

(24) Antonello, S.; Maran, F. *J. Am. Chem. Soc.* **1999**, *121*, 9668–9676.

(25) Wu, Z.; Suhan, J.; Jin, R. *J. Mater. Chem.* **2009**, *19*, 622–626.

(26) Dharmaratne, A. C.; Krick, T.; Dass, A. *J. Am. Chem. Soc.* **2008**, *130*, 13604–13605.

(27) Wu, Z.; Jin, R. *Nano Lett.* **2010**, *10*, 2568–2573.

(28) Savéant., J.-M. *J. Am. Chem. Soc.* **1987**, *109*, 6788–6795.

(29) Antonello, S.; Musumeci, M.; Wayner, D. D. M.; Maran, F. *J. Am. Chem. Soc.* **1997**, *119*, 9541–9549.

(30) Full details on the dissociative reduction of perfluorodibenzoyl peroxide, the determination of the relevant ET parameters, and its ET reaction with Au_{25} will be published elsewhere.

(31) Chateauneuf, J.; Lusztyk, J.; Ingold, K. U. *J. Am. Chem. Soc.* **1988**, *110*, 2886–2893.

(32) Lee, D.; Donkers, R. L.; Wang, G.; Harper, A. S.; Murray, R. W. *J. Am. Chem. Soc.* **2004**, *126*, 6193–6199.

(33) Parker, J. P.; Weaver, J. E. F.; McCallum, F.; Fields-Zinna, C. A.; Murray, R. W. *Langmuir* **2010**, *26*, 13650–13654.

(34) Qian, H.; Jin, R. *Nano Lett.* **2009**, *9*, 4083–4087.

(35) Qian, H.; Zhu, M.; Andersen, U. N.; Jin, R. *J. Phys. Chem. A* **2009**, *113*, 4281–4284.